

# New Insight of Pyrrole-Like Nitrogen for Boosting Hydrogen Evolution Activity and Stability of Pt Single Atoms

Lei Zhang, Qi Wang, Rutong Si, Zhongxin Song, Xiaoting Lin, Mohammad Norouzi Banis, Keegan Adair, Junjie Li, Kieran Doyle-Davis, Ruying Li, Li-Min Liu,\* Meng Gu,\* and Xueliang Sun\*

Single atomic Pt catalysts exhibit particularly high hydrogen evolution reaction (HER) activity compared to conventional nanomaterial-based catalysts. However, the enhanced mechanisms between Pt and their coordination environment are not understood in detail. Hence, a systematic study examining the different types of N in the support is essential to clearly demonstrate the relationship between Pt single atoms and N-doped support. Herein, three types of carbon nanotubes with varying types of N (pyridine-like N, pyrrole-like N, and quaternary N) are used as carbon support for Pt single atom atomic layer deposition. The detailed coordination environment of the Pt single atom catalyst is carefully studied by electron microscope and X-ray absorption spectra (XAS). Interestingly, with the increase of pyrrole-like N in the CNT support, the HER activity of the Pt catalyst also improves. First principle calculations results indicate that the interaction between the  $d_{yz}$  and  $s$  orbitals of H and  $sp^3$  hybrid orbital of N should be the origin of the superior HER performance of these Pt single atom catalysts (SACs).

the production of hydrogen fuel is from steam-reformed methane, which will cause severe climate problems due to the production of huge amount of  $CO_2$ .<sup>[5,6]</sup> Hence, the development of alternative routes for hydrogen production is significant. The electrochemical hydrogen evolution reaction (HER) is one promising route for producing clean hydrogen, which has generated significant interest during recent years.<sup>[7]</sup> In HER, platinum (Pt) exhibited better activity compared with other elements.<sup>[8–10]</sup> However, the practical application of HER is seriously hindered by the cost and limited reserves of Pt available for to catalyze the reaction. One of the most direct routes to reducing the Pt cost is to increase the atom utilization efficiency (AUE) by reducing the particle size to clusters or even single atoms catalysts.<sup>[11,12]</sup> Thus far, the Pt single

## 1. Introduction

Hydrogen is a clean fuel, and it is the key energy source in proton exchange membrane fuel cells, which have many potential applications.<sup>[1–4]</sup> Until now, the main strategy for

atom catalysts can be successfully prepared by wet impregnation techniques,<sup>[13–15]</sup> coprecipitation,<sup>[16]</sup> atomic layer deposition method (ALD),<sup>[17–20]</sup> and some other methods.<sup>[21,22]</sup>


Among the various techniques for the fabrication of single atom catalysts (SACs), ALD enables precise control over the deposition of single atoms and nanoclusters. For example, we developed a practical synthesis method to fabricate Pt single atoms on graphene nanosheets by ALD.<sup>[17]</sup> During the Pt ALD process, Pt atoms tend to bond with the active sites of the support. If the bonding energy is too weak, Pt atoms could migrate along the support, which results in the formation of clusters. Therefore, the selectivity of the support is significant for stabilizing Pt single atoms.<sup>[23,24]</sup> It has been reported that metal-N bonding is helpful for stabilizing and activating the single atoms.<sup>[25–27]</sup> For example, our group tried to load Pt single atoms and clusters on nitrogen-doped graphene, which exhibited 374 times greater HER activity than that of its commercial Pt/C counterpart.<sup>[18]</sup> However, the enhanced mechanisms between Pt and their coordination environment are not understood in detail. Recently, several studies indicated that the activity of SACs closely correlated with the N-speciation in C-based materials for catalytic applications.<sup>[28,29]</sup> A systematic study examining the different types of N in the support is essential to identify the synergistic effect between Pt single atoms and N-doped support during HER process.

Dr. L. Zhang, Dr. Z. Song, Dr. X. Lin, Dr. M. N. Banis, K. Adair, J. Li, K. Doyle-Davis, R. Li, Prof. X. Sun  
Department of Mechanical and Materials Engineering  
The University of Western Ontario  
London, ON N6A 5B9, Canada  
E-mail: xsun@eng.uwo.ca

Dr. Q. Wang, Prof. M. Gu  
Department of Materials Science and Engineering  
Southern University of Science and Technology  
Shenzhen 518055, P. R. China  
E-mail: gum@sustech.edu.cn

R. Si  
Beijing Computational Science Research Center  
Beijing 100193, China

Prof. L.-M. Liu  
School of Physics  
Beihang University  
Beijing 100083, China  
E-mail: liminliu@buaa.edu.cn

 The ORCID identification number(s) for the author(s) of this article can be found under <https://doi.org/10.1002/sml.202004453>.

DOI: 10.1002/sml.202004453

Herein, we employed three types of carbon nanotubes (CNT) with varying types of N (pyridine-like nitrogen, pyrrole-like nitrogen, and quaternary N) as carbon support for Pt single atom atomic layer deposition. We found that almost complete deposition of Pt single atoms can be obtained on high N-content carbon nanotubes (HNCNT). In addition, the detailed electronic structure of the obtained Pt SACs is studied by X-ray absorption near edge structure (XANES) and extended X-ray absorption fine spectra (EXAFS). Interestingly, we found that pyrrole-like nitrogen in the CNT support can boost the HER activity and stability of Pt single atoms. DFT calculation results indicate that the interaction between the *d<sub>yz</sub>* and *s* orbitals of H and *sp<sup>3</sup>* orbital of N should be the origin of the superior HER performance of Pt SACs.

## 2. Results and Discussion

In order to investigate the relationship between Pt ALD and incorporated nitrogen concentration in the substrate, we employed commercial CNT and two types of melamine-derived N-doped CNT as the substrates (denoted hereafter as CNT, NCNT, and HNCNT). Figure S1 (Supporting Information) shows typical TEM images of the three types of carbon nanotubes with differing N contents. It can be clearly observed that the roughness and density of bamboo-like structures tend to increase with N content.<sup>[30]</sup> X-ray photoelectron spectroscopy (XPS) results indicate that the N contents in the CNT, NCNT, and HNCNT are 1.7%, 3.6%, and 9.4%, respectively (Figure 1a and Table S1, Supporting Information). The fitted peaks of the C 1s spectral components at bond energies of 284.5, 285, and 286.8 eV correspond to the C–C bonds, C–C structural defects, and C=O chemical bonds, respectively.<sup>[31]</sup> It should be pointed out that with an increase in N doping, the ratio of the C–C defect peak increased from 9.7% to 27.7 and 36.9%, which indicates that N-doping is helpful for the creation of defects on the carbon supports (Figure 1b,c,e). The defects are also beneficial to stabilize Pt single atoms from aggregation. The asymmetric N 1s spectra can be fitted into six peaks at 398.2 eV (N1), 399.8 eV (N2), 401.0 eV (N3), 402.0 eV (N4), 403.9 eV (N5), and 405.0 eV (N6) (Figure 1d,f). The peaks at 398.2, 399.8, and 401.0 eV are attributed to pyridine-like nitrogen, pyrrole-like nitrogen, and quaternary N, respectively.<sup>[32]</sup> The peaks N3, N4, and N5 are attributed to the triply coordinated configuration, with oxidized nitrogen and molecular nitrogen inside the cavities of the nanotubes.<sup>[33]</sup> It should be noted that the amount of pyrrole-like nitrogen in HNCNT is much more than that in NCNT. The ratio of pyrrole-like nitrogen to pyridine-like nitrogen is close to 1:1 in HNCNT, while the ratio in NCNT is only around 1:3. This result indicated that the pyrrole-like nitrogen exists widely in HNCNT structure. In addition, we used Raman spectroscopy to further investigate the physical properties of the as-prepared carbon nanotubes. Figure S2 (Supporting Information) presents the Raman spectra obtained for the CNTs with different N content. A typical D band peak located at 1350  $\text{cm}^{-1}$  and a G band peak located at 1580  $\text{cm}^{-1}$  can be observed for all samples. The band intensity ratio ( $I_D/I_G$ ) is highly dependent on the defect density of the nanotubes, with higher ratios corresponding to more defects.<sup>[34,35]</sup> In our case,

the  $I_D/I_G$  ratio for CNT, NCNT, and HNCNT is 0.64, 0.74, and 1.08, respectively. In addition, the 2D peak at around 2695  $\text{cm}^{-1}$  gradually decreased with the increase of N, which might due to the increase of number of layers of nanotube and the introduction of N.<sup>[36,37]</sup> This result indicates that the graphitic carbon structure is modified with the doping of N. In particular, when the N content in CNT increased from 3.6% to 4.4%, there is a gradual increase in the number of defects.

ALD synthesis of Pt atoms on CNT, NCNT, and HNCNT was prepared by dosing MeCpPtMe<sub>3</sub> for 30 s time in the chamber. After the reaction, Pt clusters with the average size of 1 nm (Figure S3, Supporting Information) formed on CNT (denoted hereafter as Pt-CNT). Due to the weak bonding energy of Pt–C, Pt atoms can migrate on the support, which results in the formation of clusters. We carried out the same ALD procedure to deposit Pt atoms on NCNT and HNCNT. The Pt atoms prefer to absorb and bond with the N atoms on NCNT and HNCNT, creating strong metal–support interactions between Pt single atoms and N-doping sites. From low resolution transmission electron microscopy (TEM) and STEM images (Figure 2a and Figure S4a, Supporting Information), no nanoscale clusters formed on either NCNT or HNCNT (denoted hereafter as Pt-NCNT and Pt-HNCNT). We further characterized the two samples by aberration-corrected high angle annular dark field scanning transmission electron microscopy (AC-HAADF-STEM). As shown in Figure S4 (Supporting Information), numerous individual Pt atoms are uniformly dispersed on the NCNTs. When deposited on HNCNT, due to the abundant N-doping sites and defects, most of Pt exhibited as isolated single atoms (Figure 2b). Interestingly, we found that Pt atoms were preferentially deposited in N-rich region; while in the regions without N sites, few Pt atoms can be found (Figure 2c,d; Figure S5, Supporting Information). As we discussed in the XPS characterization, the N might be pyrrolic and pyridinic N and quaternary N. Due to the geometric effect, the pyrrolic and pyridinic N can anchor Pt single atoms more easily compared with quaternary N on HNCNT. Therefore, the N-rich area might be due to the thick HNCNT and would abundant pyrrolic or pyridinic N, which are helpful for trapping the Pt single atoms. Elemental mapping analysis (Figure 2e) demonstrates that the Pt SACs are well dispersed on the HNCNT substrate. Inductively coupled plasma-optical emission spectrometer (ICP-OES) results show that the Pt loading after ALD is 0.9 wt%. Furthermore, we tried to load the same Pt loading by impregnation method.<sup>[38]</sup> The detailed method is shown in the experimental part. As shown in Figure S6 (Supporting Information), several clusters with the size of 1 nm formed on the HNCNT, indicating that the Pt–Pt bond formed during the preparation process. When compared with impregnation method, ALD method can effectively avoid the formation of Pt–Pt bond and obtain well-dispersed Pt single atoms on this HNCNT substrate.

We carried out XANES and EXAFS measurements to further investigate the coordination environment of Pt atoms on CNT, NCNT, and HNCNT. Figure 3a shows that the Pt-HNCNT have the most intense white line (WL) compared to Pt-NCNT, Pt-CNT, and Pt foil. The area under the WL peak of Pt *L<sub>3</sub>*-edge X-ray absorption spectra is directly related to the unoccupied state density of the Pt 5d orbitals. Usually, the number of vacancies in the occupied d band increases with the increase in the *L<sub>3</sub>*-edge intensity. In addition, several studies show that the vacant d-orbitals

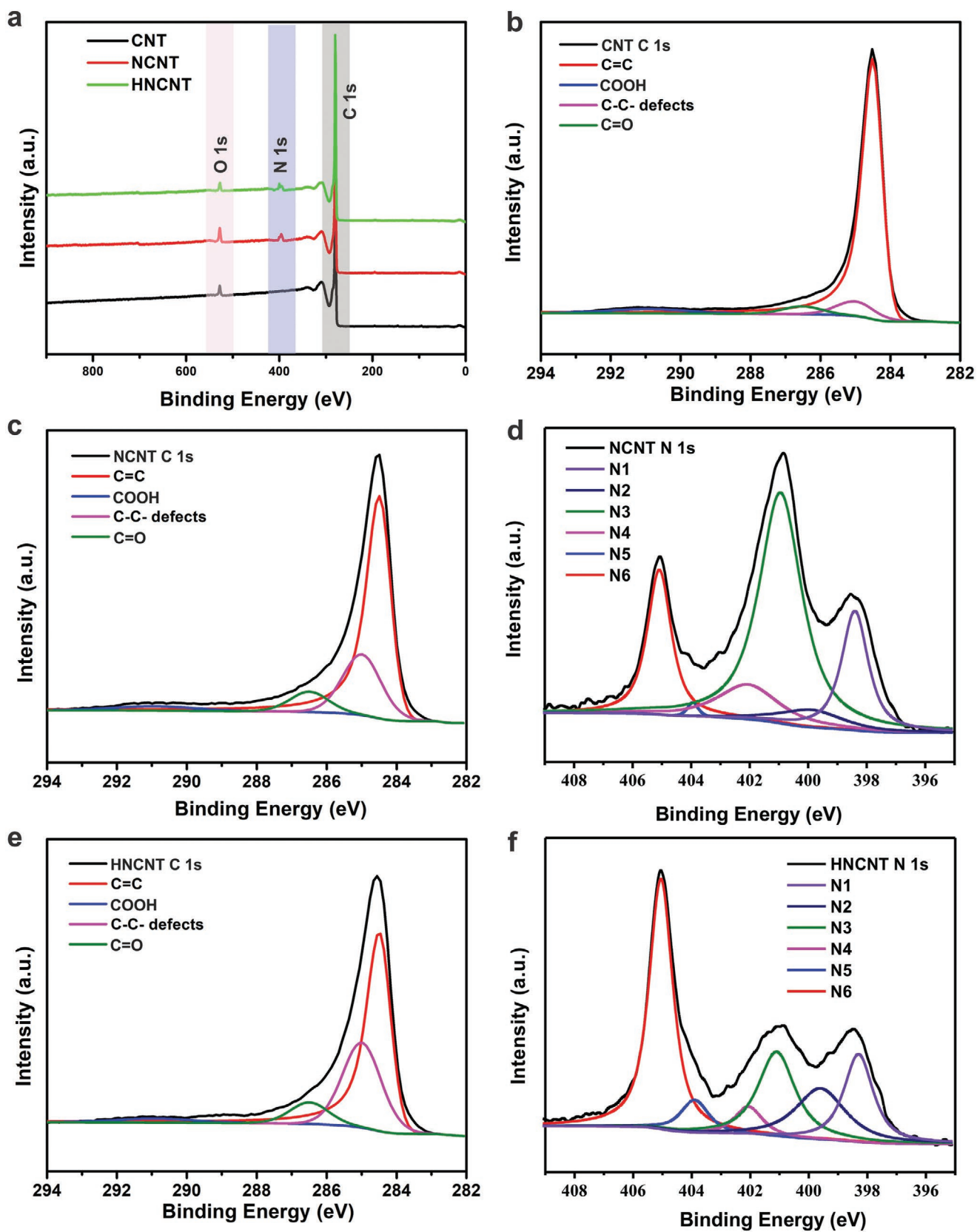


**Figure 1.** a) Survey XPS spectra for CNT, NCNT, and HNCNT samples. b) XPS spectra of C 1s for CNT sample. c,d) XPS spectra of C 1s and N 1s for NCNT. e,f) XPS spectra of C 1s and N 1s for HNCNT.



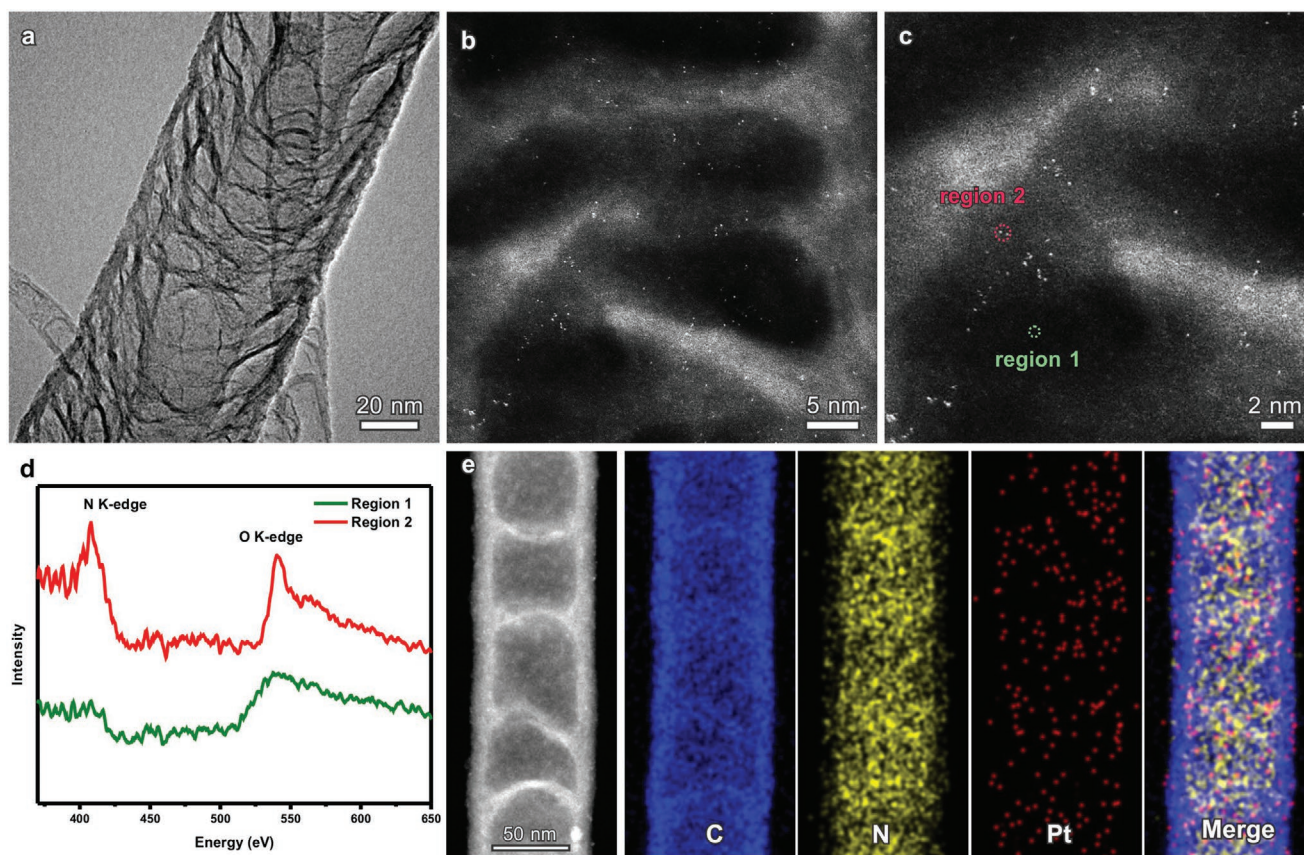


**Figure 2.** a) The typical TEM images of Pt-HNCNT. b,c) Atomic-resolution STEM image of Pt-HNCNT, showing the formation of Pt single atoms. d) The EELS spectra obtained from two different regions shown in (c). e) HAADF-STEM image and corresponding HAADF-STEM-EDS elemental mapping of Pt-HNCNT.

of Pt atoms can significantly affect their catalytic activities.<sup>[18,19]</sup> Besides the intensity, a small positive shift in the threshold energy  $E_0$  can be observed for the Pt atoms on the three CNT supports compared to Pt foil. Among the three samples, the  $E_0$  for Pt-NCNT and Pt-HNCNT are 11 565.7 and 11 566.0 eV, which means Pt single atoms are positively charged when they bonded with N. With the formation nanoparticles on CNTs, the  $E_0$  changed to 11 564.8 eV. This result indicate that Pt exhibited relatively more metallic property with the formation of nanoparticles.

Furthermore, we analyzed the Fourier transforms EXAFS spectra of Pt to investigate the local atomic structure of Pt, which were plotted in Figure 3b. The peak at 1.6 Å is attributed to Pt bonded to carbon or nitrogen, and the peak at 2.6 Å is associated with the Pt–Pt. For the Pt foil, a peak located at 2.6 Å can be observed. The Pt-CNT exhibited two peaks at 1.6 and 2.6 Å. While for the Pt-NCNT and Pt-HNCNT catalysts, only a peak at 1.6 Å is observed, indicating the formation of single atom structure. Furthermore, the detailed coordination information of Pt–C, Pt–N and Pt–Pt was quantitatively analyzed by fitting the EXAFS curves (Figure 3c–f). As shown in Table 1, the Pt single atoms on HNCNT and NCNT have the coordination numbers (CN) of 2.3 and 1.2 for Pt–C and Pt–N bonding respectively. In addition, we found a Pt–Pt CN of 6.2 and a Pt–C CN of 4.5 for the Pt-CNT, which supports the formation of single atoms and nanoparticles on Pt-CNT sample.

Cyclic voltammograms (CV) were recorded in 0.5 M  $\text{H}_2\text{SO}_4$  at a scanning rate of 50  $\text{mV s}^{-1}$ . We can clearly observe the hydrogen adsorption/desorption peak for the Pt-CNT and Pt/C catalysts due to the presence of Pt–Pt bond. Due to the formation of Pt single atoms on NCNT and HNCNT, we cannot observe the hydrogen adsorption/desorption peak (Figure S7, Supporting Information). The HER activity of the Pt-CNT, Pt-NCNT and Pt-HNCNT was measured in comparison to a commercial Pt/C catalyst. The polarization curves show that the Pt-HNCNT exhibited better HER performance compared with Pt-CNT and Pt-NCNT (Figure 4a). The specific activity for each catalyst was calculated from the polarization curves by normalizing the current with the geometric area of the electrode (Figure 4b). The Pt-HNCNT exhibited comparable specific activity with Pt/C. In addition, the Pt-HNCNT catalyst needs a lower overpotential of  $\approx 15$  mV to achieve a current density of 10  $\text{mA cm}^{-2}$  for HER. When normalized to the metal loading, the mass HER activities for the Pt-HNCNT and Pt-NCNT at the overpotential of 0.05 V are 20.4 and 10.3  $\text{A mg}^{-1}$ , which are 47 and 23 times greater than that of the commercial Pt/C catalyst (0.43  $\text{A mg}^{-1}$ ). These results indicate that the HNCNT structures can significantly improve the HER activity of Pt when compared with NCNT and regular CNT substrates.

We calculated the Tafel plots to illustrate the HER kinetics (Figure S8, Supporting Information). The Tafel slope of

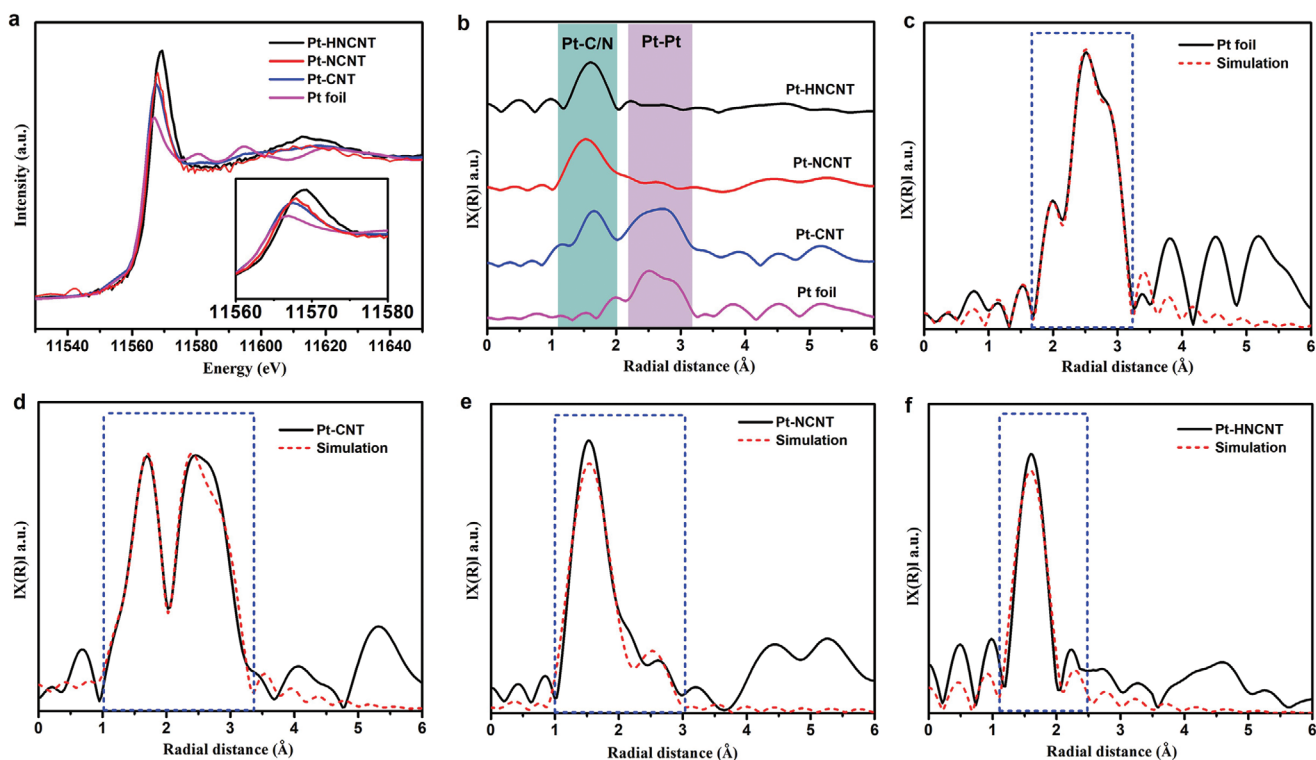


**Figure 3.** X-ray absorption studies of the Pt-CNT, Pt-NCNT, Pt-HNCNT, and Pt foil. a) The normalized XANES spectra at the Pt L3-edge of the Pt-CNT, Pt-NCNT, Pt-HNCNT, and Pt foil. b) Corresponding K3-weighted Fourier transform spectra from EXAFS of the Pt-CNT, Pt-NCNT, Pt-HNCNT, and Pt foil. c–f) EXAFS fitting in Pt R-space for the samples: Pt-CNT, Pt-NCNT, Pt-HNCNT, and Pt foil.

Pt-HNCNT and Pt/C was 29.1 and 29.7 mV dec<sup>-1</sup>, respectively. Although the Tafel slope for SACs and NPs are close, the HER process might be different due to the different coordination environment of SA and NPs. On Pt NPs, during the first step of HER, an adsorbed hydrogen atom formed at the Pt surface. The second hydrogen atom tend to be adsorbed on the neighboring Pt atom. Then these two adsorbed H atoms form molecular hydrogen (Tafel reaction). For the Pt single atom catalysts, it has been reported that several H could adsorb on one Pt atom, followed by the formation of H<sub>2</sub> on the isolated Pt atom.<sup>[39,40]</sup> The desorption process is similar as the Tafel reaction (H<sub>ads</sub> + H<sub>ads</sub> → H<sub>2</sub>), which results in the similar Tafel slope. To evaluate the durability of the as-prepared Pt-HNCNT, accelerated

degradation tests (ADTs) were carried out between +0.4 and -0.15 V (vs RHE) at 100 mV s<sup>-1</sup> for 5000 cyclic voltammetry sweeps. As shown in Figure 4c,d, the Pt-HNCNT catalysts exhibited very good stability, and the current density at overpotential of 0.05 V maintained 88% after 5000 cycles ADT test. While for the commercial Pt/C catalyst, the current density dropped to 72% after 5000 cycles at an overpotential of 0.05 V (Figure S9, Supporting Information). The good stability of Pt single atoms on HNCNT was originated from the strong Pt–N interaction.

We performed density functional theory (DFT) calculations to systematically understand the origin of the HER activity of Pt single atoms (SAs) on HNCNT. Unlike Pt nanoparticles (NPs),<sup>[18]</sup> each Pt single atom can adsorb more than one

**Table 1.** XAS analysis results for the Pt-CNT, Pt-NCNT, Pt-HNCNT and Pt foil.

Sample	Pt L <sub>3</sub> edge WL		Path	Coordination number	Bond length [Å]	Δ <sup>2</sup> 10 <sup>-3</sup> Å <sup>2</sup>
	E <sub>0</sub> [eV]	E <sub>Peak</sub> [eV]				
Pt foil	11 564	11 566.6	Pt–Pt	12	2.76	4.7
Pt-CNT	11 564.8	11 567.4	Pt–Pt	6.2	2.74	7.4
			Pt–C	4.5	2.07	7.8
Pt-NCNT	11 565.7	11 567.9	Pt–N	1.2	1.93	2.1
			Pt–C	2.3	2.04	1.6
Pt-HNCNT	11 566.0	11 569.1	Pt–N	1.2	1.93	3.0
			Pt–C	2.0	2.01	1.1

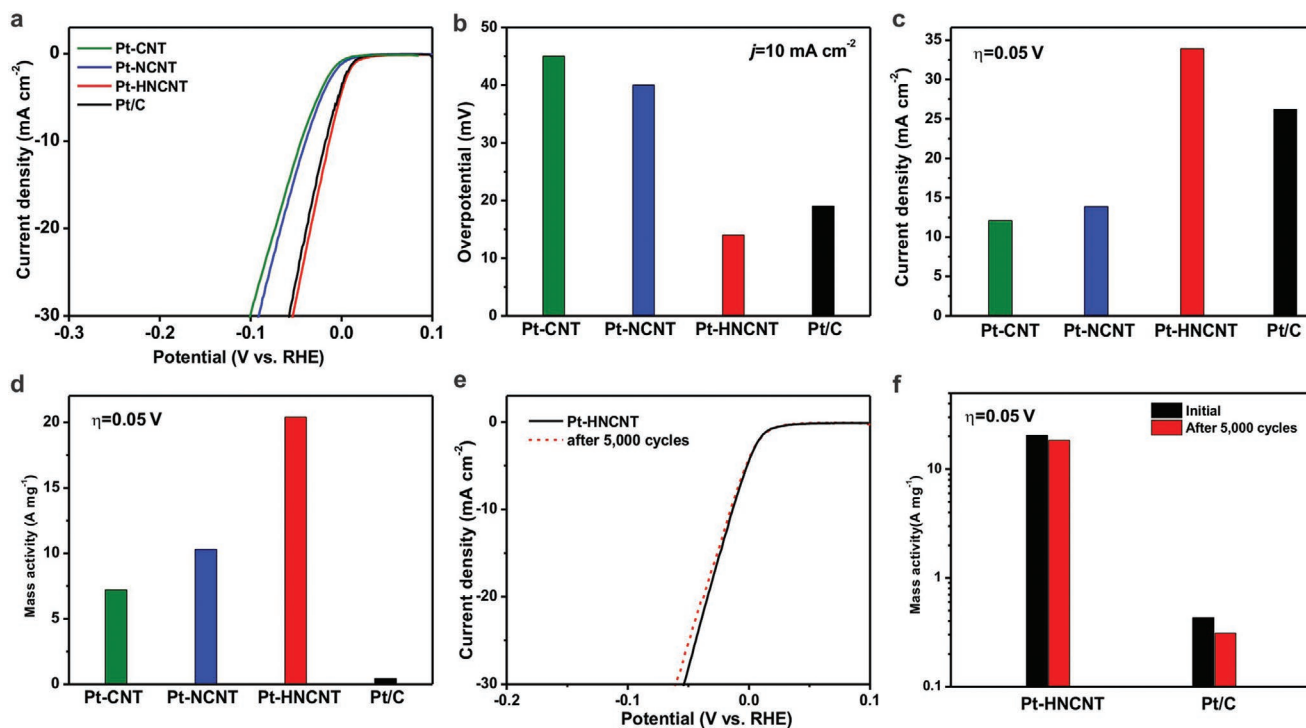


**Figure 4.** a) The HER polarization curves recorded on Pt-CNT, Pt-NCNT, Pt-HNCNT, and Pt/C catalysts. b) The required overpotential to reach the current density of 10 mA cm<sup>-2</sup>. c) The specific current densities at 0.05 V, which were normalized to the geometric area of the RDE (0.196 cm<sup>2</sup>) of Pt-CNT, Pt-NCNT, Pt-HNCNT, and Pt/C catalysts. d) Normalized mass activity at 0.05 V of Pt-CNT, Pt-NCNT, Pt-HNCNT, and Pt/C catalysts. e) Durability measurement of the Pt-HNCNT catalysts. f) Normalized mass activity at 0.05 V of Pt-HNCNT and Pt/C catalysts before and after durability tests.

H atom. Our previous work revealed that each Pt SAs could adsorb up to four H atoms and the best HER performance of Pt SAs is presented at the last step of H atom adsorption evolution.<sup>[19]</sup> It should be noticed that the primary nitrogen species in Pt-HNCNT is pyridine and pyrrole-like N. To systematically examine how hydrogen evolves in HER process, the Pt-HNCNT and Pt-NCNT are deeply compared. In the following, we referred the model for Pt-NCNT and Pt-HNCNT in our calculation as A and B (Figure 5a).

Calculations of hydrogen adsorption Gibbs free energy ( $\Delta G_{\text{H}}$ ) of Pt-HNCNT were performed to examine the HER activity (Figure 5b). The  $\Delta G_{\text{H}}$  of Pt-HNCNT gradually decreases as the number of adsorbed hydrogens increased. Considering the smallest  $\Delta G_{\text{H}}$  reaches at the highest hydrogen convergence (B-4H), the corresponding oxidation states of Pt atom and orbital interactions between Pt, N, and H atom are studied based on the PDOS. Before the Pt SA reaches the best HER activity on B, one hydrogen atom heads to the  $d_{x^2-y^2}$  and two hydrogens head to  $d_{xy}$  and  $d_{xz}$ . The hybridization of the N atom in the pyrrole ring is mainly  $sp^3$ . On this occasion, the  $d_{xy}$ ,  $d_{yz}$ , and  $d_{xz}$  are half-filled. The  $d_{x^2-y^2}$  and  $d_z^2$  are fully occupied. Here, the hydrogen of the smaller  $\Delta G_{\text{H}}$  stays primarily in the direction of  $d_{xz}$ .

After one more hydrogen is adsorbed on the Pt SA, the Pt atom is reduced by the hydrogen from 3+ to 2+, the corresponding oxidation state for Pt are explored based on PDOS and occupation number<sup>[41]</sup> (Table S2, Supporting Information). The hydrogen heads to the  $d_{yz}$  orbital. In this process, the hybridization of N atom is still  $sp^3$  and the hybrid orbital tends to be more localized (see Figure S10 in the Supporting Information),

the s orbital of the absorbed hydrogen atom interacts with the  $sp^3$  orbital of the N atom in the pyrrole ring and then forms bonding and antibonding orbitals (Figure 6a,b). Meanwhile, the  $d_{x^2-y^2}$  and  $d_z^2$  remain fully occupied, the  $d_{xy}$  and  $d_{xz}$  become fully occupied and  $d_{yz}$  becomes fully unoccupied (Figure 6c). The  $d_{yz}$  orbital changes from half-occupied to fully unoccupied, interacting with the bonding orbital of H and N atom. Then the antibonding orbital of H and N atom interacts with  $d_{x^2-y^2}$  of Pt atom, which introduces an antibond (Figure 6b). The hydrogen atom showing the smallest  $\Delta G_{\text{H}}$  on the Pt atom heads to the  $d_{x^2-y^2}$  orientation. The  $d_{yz}$  orbital of Pt SA interacts with the bonding orbital of H and N atom, then the  $d_{x^2-y^2}$  orbital of Pt SA interacts with the antibonding orbital of H and N atom (Figure 6b). This is stemmed from adsorbate orbital induced effects. Due to the antibonding orbital including  $d_{x^2-y^2}$  orbital of Pt atom and s orbital of H atom,  $sp^3$  hybridized orbital is pushed to a rather high energy level by the adsorbate orbital induced effect during the hydrogen adsorption (Figure 6d). The interaction between s orbital of H atom and  $d_{x^2-y^2}$  orbital of Pt SA should be quite weak. This is the main reason for the superior HER performance exhibited by the Pt-HNCNT in our experiment.

### 3. Conclusion

We have successfully prepared high quality of Pt single atoms on HNCNT through an ALD process. The as-prepared Pt single atoms on HNCNT with high content of pyrrole-like nitrogen showed much higher mass activity (47 times) and excellent



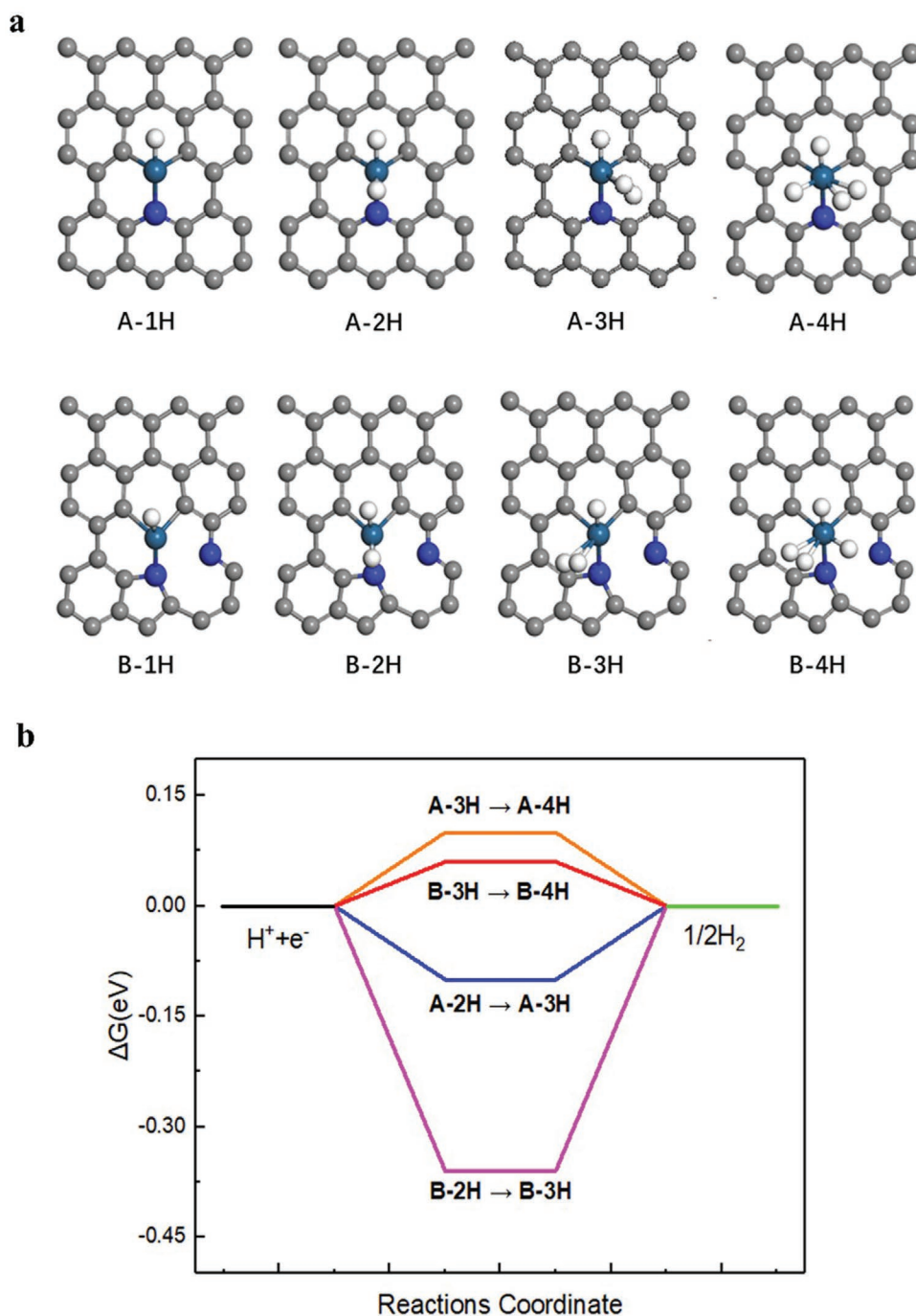


**Figure 5.** a) The structure of A and B Pt-HNCNT with the different coverages of hydrogen, respectively. b) The hydrogen adsorption Gibbs free energy of A and B Pt-HNCNT with the maximum and secondary maximum hydrogen adsorption, respectively.

stability compared to commercial Pt/C catalysts for HER. We investigate the coordination environment of Pt on CNT, NCNT and HNCNT by X-ray absorption fine spectra. Furthermore, the first-principles calculation reveals that with the adsorbate orbital induced effect of the hydrogen, the interaction between  $d_{yz}$  and s orbital of H and  $sp^3$  hybrid orbital of N results in the high HER activity. This work provides a new avenue for developing high quality single atom catalysts for electrocatalytic reactions

and brings new understanding about catalytic performances of single atom catalysts.

#### 4. Experimental Section

*Synthesis of NCNT and HNCNT with Different N Content:* The commercial CNTs used in this paper was phased from Shenzhen Nanotech Port Co. Ltd. NCNTs with a diameter range of 100nm were

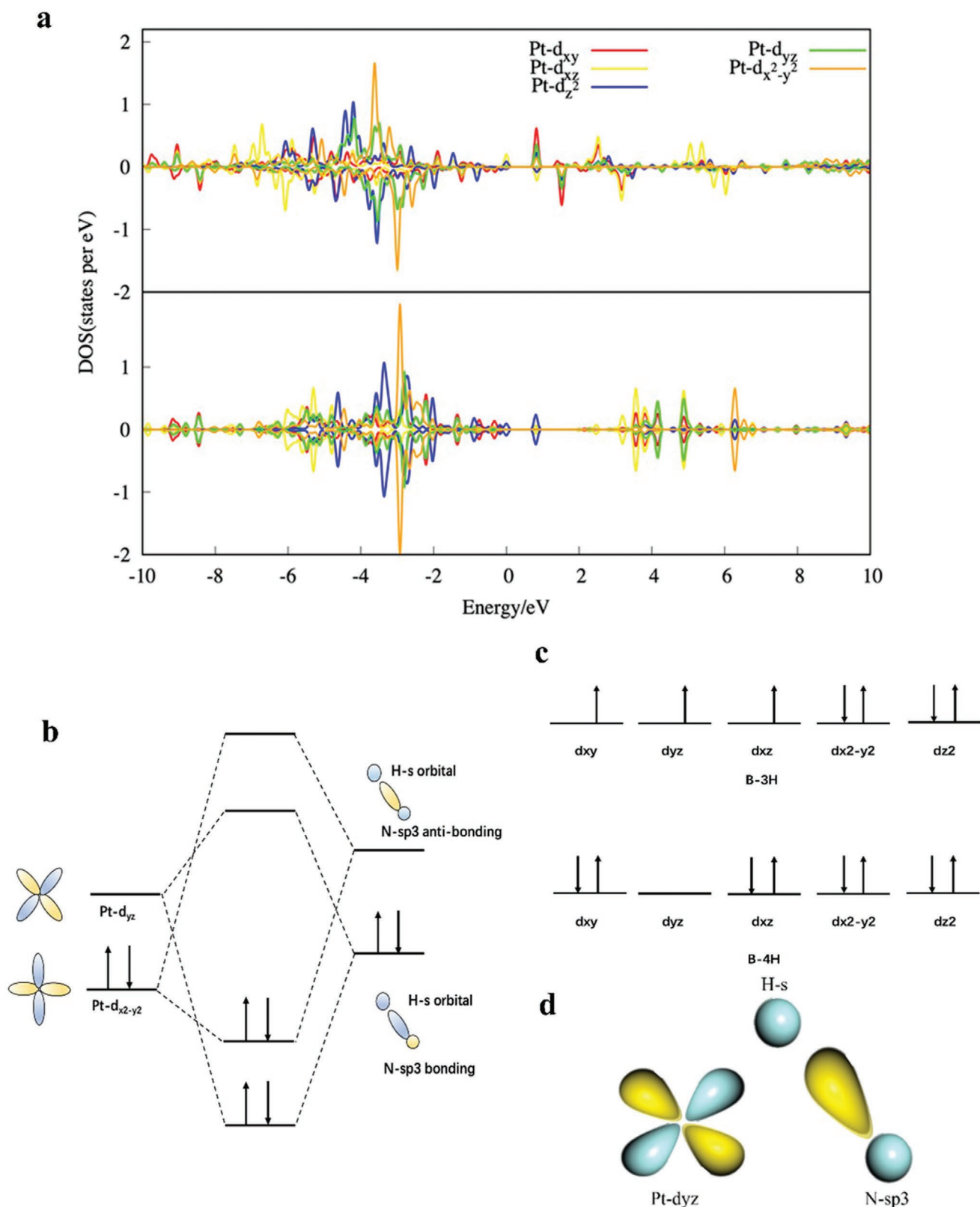


**Figure 6.** a) Upper is the PDOS (partial density of states) of Pt-HNCNT with the adsorption of three hydrogen. Lower is the PDOS (partial density of states) of Pt-HNCNT with the adsorption of four hydrogen. b) The schematic of the molecular orbital interaction of Pt, N and H atom. c) Schematic of d electron configuration of Pt of B-3H and B-4H. d) The schematic of the interaction of the  $d_{yz}$  orbital of Pt atom and the hydrogen atom of hydrogen and the  $sp^3$  orbital of nitrogen atom.



prepared by ultrasonic spray pyrolysis as outlined previously.<sup>[42]</sup> The preparation of HNCNTs was carried out by modifying a previously reported protocol.<sup>[43]</sup> The HNCNTs were prepared with Fe/Al alloy catalyst, Ni foam as the NCNTs support, melamine as the C and N sources via the floating-catalyst chemical vapor deposition (CVD) method. The received NCNTs and HNCNTs were washed with nitric acid and water for 6 h at 80 °C, respectively. The NCNTs were loaded on aluminum foil before putting into the ALD reactor chamber.

**ALD Synthesis of Pt Single Atoms or Nanoparticles on CNTs with Different N Content:** Trimethyl(methylcyclopentadienyl)-platinum (IV) (MeCpPtMe<sub>3</sub>) was used as precursor for the preparation of Pt SACs on the three types of CNTs with different N content at 250 °C by ALD (Savannah 100, Cambridge Nanotechnology Inc., USA). The purging gas and carrier gas is high-purity N<sub>2</sub> (99.9995%). The container for MeCpPtMe<sub>3</sub> was kept at 65 °C to provide a steady-state flux of Pt to the reactor. The ALD of Pt atoms were proceeded by a 30 s exposure of Pt precursor. Gas lines were held at 150 °C to avoid precursor condensation. The samples for ICP-OES test were dissolved in hot fresh aqua regia and filtered. As comparison, Pt was tried to deposit on the HNCNT by impregnation method as outlined previously.<sup>[38]</sup> 50 mg HNCNT was used as the carbon substrate and dispersed in 80 mL distilled water. Then 1 mL of H<sub>2</sub>PtCl<sub>6</sub>·6H<sub>2</sub>O solution (2 mg mL<sup>-1</sup>) was added dropwise, followed by stirring at 70 °C for 10 h. The product was washed with water and ethanol, and drying at 70 °C overnight.

**Electrochemical Measurements:** The electrochemical measurements were performed in a three-electrode system according to a previously reported protocol.<sup>[19]</sup> The working electrode was prepared by loading the ink (20 μL, 1.5 mg mL<sup>-1</sup>) on the glassy carbon rotating disk electrode. The HER test was carried out in an N<sub>2</sub>-saturated 0.5 M H<sub>2</sub>SO<sub>4</sub> at room temperature with a scan rate of 2 mV s<sup>-1</sup>. During the HER tests, the working electrode was rotated at 1600 r.p.m. to remove the H<sub>2</sub> gas bubbles formed at the catalyst surface.

**Instrumentation:** The TEM work was carried out using an aberration-corrected FEI Titan 80-300 operating at 300 kV equipped with an X-FEG gun and Bruker Super-X EDX detectors. The STEM-EDX mapping was obtained with a beam current of ≈1 nA and counts up to 6k cps for ≈5 min. The X-ray absorption spectroscopy test for the Pt single atoms was carried out at Canadian Light Source using the hard X-ray microanalysis (HXMA) beamline in fluorescence mode. The spectra of high purity Pt metal foil were collected in transmission mode for comparison and monochromatic energy calibration. The obtained XAS data were analyzed using Athena software. The extracted EXAFS data was weighted by k<sup>3</sup> to obtain the magnitude plots of the EXAFS spectra in radial space. The data was fit using Artemis software.

**Computational Method:** First-principles calculations were performed by the CP2K/Quickstep package.<sup>[44]</sup> The nonlocal exchange and correlation energies were described by the Perdew-Burke-Ernzerhof functional.<sup>[45]</sup> The core electrons is described by the nonconserving Goedecker, Teter, and Hutter (GTH) pseudopotentials.<sup>[46]</sup> Gaussian function with molecularly optimized double-zeta polarized basis sets (m-DZVP) were used for expanding the wave function of N 1s<sup>2</sup>2s<sup>2</sup>2p<sup>3</sup> and C 1s<sup>2</sup>2s<sup>2</sup>2p<sup>2</sup>, and triple-zeta polarized basis sets (m-TZVP) for Pt 4s<sup>2</sup>4p<sup>6</sup>5d<sup>9</sup>6s<sup>1</sup> electrons.<sup>[47]</sup> The cutoff energy of auxiliary basis set of plane waves is 500 Ry. During the calculations, all the atomic positions were fully relaxed until the force is smaller than 0.05 eV Å<sup>-1</sup>. The hydrogen-adsorption Gibbs free energies, ΔG<sub>H</sub>, were calculated by the following equations<sup>[48]</sup>

$$\Delta E_{\text{H}} = E_{(n+1)\text{H}/\text{Pt}} - E_{n\text{H}/\text{Pt}} - 1/2E_{\text{H}_2} \quad (1)$$

$$\Delta G_{\text{H}} = \Delta E_{\text{H}} + \Delta E_{\text{ZPE}} - T\Delta S \quad (2)$$

ΔE<sub>H</sub> is defined as the hydrogen binding energy on metal atoms. E<sub>(n+1)H/Pt</sub> and E<sub>nH/Pt</sub> refer to the total energies of n+1 and n hydrogen atoms adsorbed on Pt atom. E<sub>H<sub>2</sub></sub> refers to the total energy of a hydrogen molecule in vacuum. ΔE<sub>ZPE</sub> is the difference of the zero-point energy with and without hydrogen adsorption, T is the temperature, 300 K, and ΔS is the entropy change between an adsorbed hydrogen and gas-phase hydrogen at 101 325 Pa.

## Supporting Information

Supporting Information is available from the Wiley Online Library or from the author.

## Acknowledgements

L.Z., Q.W., and R.S. contributed equally to this work. This work was supported by Natural Sciences and Engineering Research Council of Canada (NSERC), Canada Research Chair (CRC) Program, Canada Foundation for Innovation (CFI), and the University of Western Ontario. We were also supported by the Science Challenge Project (TZ2018004), the Fundamental Research Funds for the Central Universities, the National Natural Science Foundation of China (grant nos. 51861130360, 51572016, 11974037, 22075203, 21802065, and U1530401), and Newton Advanced Fellowships under the grant No. NAF\R1\180242, the computation supports from Tianhe-2JK computing time award at the Beijing Computational Science Research Center (CSRC).

## Conflict of Interest

The authors declare no conflict of interest.

## Keywords

atomic layer deposition, density functional theory calculations, hydrogen evolution reaction, platinum, single atoms, XAS analysis

Received: July 23, 2020

Revised: October 2, 2020

Published online:

- [1] G. W. Crabtree, M. S. Dresselhaus, M. V. Buchanan, *Phys. Today* **2004**, 57, 39.
- [2] K. M. K. Yu, W. Tong, A. West, K. Cheung, T. Li, G. Smith, Y. Guo, S. C. E. Tsang, *Nat. Commun.* **2012**, 3, 1230.
- [3] L. Zhang, K. Doyle-Davis, X. Sun, *Energy Environ. Sci.* **2019**, 12, 492.
- [4] L. Zhang, Z.-J. Zhao, M. N. Banis, L. Li, Y. Zhao, Z. Song, Z. Wang, T.-K. Sham, R. Li, M. Zheng, J. i. Gong, X. Sun, *J. Mater. Chem. A* **2018**, 6, 24397.
- [5] I. Chorkendorff, J. W. Niemantsverdriet, *Concepts of Modern Catalysis and Kinetics*, Wiley-VCH, Weinheim **2003**.
- [6] Q. Ming, T. Healey, L. Allen, P. Irving, *Catal. Today* **2002**, 77, 51.
- [7] R. Subbaraman, D. Tripkovic, D. Strmcnik, K.-C. Chang, M. Uchimura, A. P. Paulikas, V. Stamenkovic, N. M. Markovic, *Science* **2011**, 334, 1256.
- [8] H. Yin, S. Zhao, K. Zhao, A. Muqsit, H. Tang, L. Chang, H. Zhao, Y. Gao, Z. Tang, *Nat. Commun.* **2015**, 6, 6430.
- [9] S. Ye, F. Luo, Q. Zhang, P. Zhang, T. Xu, Q. Wang, D. He, L. Guo, Y. Zhang, C. He, X. Ouyang, M. Gu, J. Liu, X. Sun, *Energy Environ. Sci.* **2019**, 12, 1000.
- [10] J. Kye, M. Shin, B. Lim, J.-W. Jang, I. Oh, S. Hwang, *ACS Nano* **2013**, 7, 6017.
- [11] M. Shao, A. Peles, K. Shoemaker, *Nano Lett.* **2011**, 11, 3714.
- [12] M. Nesselberger, S. Ashton, J. C. Meier, I. Katsounaros, K. J. J. Mayrhofer, M. Arenz, *J. Am. Chem. Soc.* **2011**, 133, 17428.
- [13] S. Yang, J. Kim, Y. J. Tak, A. Soon, H. Lee, *Angew. Chem., Int. Ed.* **2016**, 55, 2058.
- [14] X. Li, W. Bi, L. Zhang, S. Tao, W. Chu, Q. Zhang, Y. Luo, C. Wu, Y. Xie, *Adv. Mater.* **2016**, 28, 2427.

- [15] J. Liu, M. Jiao, L. Lu, H. M. Barkholtz, Y. Li, Y. Wang, L. Jiang, Z. Wu, D.-J. Liu, L. Zhuang, C. Ma, J. Zeng, B. Zhang, D. Su, P. Song, W. Xing, W. Xu, Y. Wang, Z. Jiang, G. Sun, *Nat. Commun.* **2017**, *8*, 15938.
- [16] B. Qiao, A. Wang, X. Yang, L. F. Allard, Z. Jiang, Y. Cui, J. Liu, J. Li, T. Zhang, *Nat. Chem.* **2011**, *3*, 634.
- [17] S. Sun, G. Zhang, N. Gauquelin, N. Chen, J. Zhou, S. Yang, W. Chen, X. Meng, D. Geng, M. Banis, R. Li, S. Ye, S. Knights, G. Botton, T.-K. Sham, X. Sun, *Sci. Rep.* **2013**, *3*, 1775.
- [18] N. Cheng, S. Stambula, D. Wang, M. Banis, J. Liu, A. Riese, B. Xiao, R. Li, T.-K. Sham, L. Liu, G. Botton, X. Sun, *Nat. Commun.* **2016**, *7*, 13638.
- [19] L. Zhang, R. Si, H. Liu, N. Chen, Q. Wang, K. Adair, Z. Wang, J. Chen, Z. Song, J. Li, M. N. Banis, R. Li, T.-K. Sham, M. Gu, L.-M. Liu, G. A. Botton, X. Sun, *Nat. Commun.* **2019**, *10*, 4936.
- [20] H. Yan, Y. Lin, H. Wu, W. Zhang, Z. Sun, H. Cheng, W. Liu, C. Wang, J. Li, X. Huang, T. Yao, J. Yang, S. Wei, J. Lu, *Nat. Commun.* **2017**, *8*, 1070.
- [21] H. Li, L. Wang, Y. Dai, Z. Pu, Z. Lao, Y. Chen, M. Wang, X. Zheng, J. Zhu, W. Zhang, R. Si, C. Ma, J. Zeng, *Nat. Nanotechnol.* **2018**, *13*, 411.
- [22] Y. Pan, R. Lin, Y. Chen, S. Liu, W. Zhu, X. Cao, W. Chen, K. Wu, W. C. Cheong, Y. Wang, L. Zheng, J. Luo, Y. Lin, Y. Liu, C. Liu, J. Li, Q. Lu, X. Chen, D. Wang, Q. Peng, C. Chen, Y. Li, *J. Am. Chem. Soc.* **2018**, *140*, 4218.
- [23] Z. Lu, B. Wang, Y. Hu, W. Liu, Y. Zhao, R. Yang, Z. Li, J. Luo, B. Chi, Z. Jiang, M. Li, S. Mu, S. Liao, J. Zhang, X. Sun, *Angew. Chem., Int. Ed.* **2019**, *58*, 2622.
- [24] P. Chen, T. Zhou, L. Xing, K. Xu, Y. Tong, H. Xie, L. Zhang, W. Yan, W. Chu, C. Wu, Y. Xie, *Angew. Chem., Int. Ed.* **2017**, *56*, 610.
- [25] A. Han, W. Chen, S. Zhang, M. Zhang, Y. Han, J. Zhang, S. Ji, L. Zheng, Y. Wang, L. Gu, C. Chen, Q. Peng, D. Wang, Y. Li, *Adv. Mater.* **2018**, *30*, 1706508.
- [26] C. Zhu, S. Fu, J. Song, Q. Shi, D. Su, M. H. Engelhard, X. Li, D. Xiao, D. Li, L. Estevez, D. Du, Y. Lin, *Small* **2017**, *13*, 1603407.
- [27] X. Liu, Y. Sui, T. Duan, C. Meng, Y. Han, *Catal. Sci. Technol.* **2015**, *5*, 1658.
- [28] S. K. Kaiser, E. Fako, G. Manzocchi, F. Krumeich, R. Hauert, A. H. Clark, O. V. Safonova, N. López, J. Pérez-Ramírez, *Nat. Catal.* **2020**, *3*, 376.
- [29] S. K. Kaiser, R. Lin, S. Mitchell, E. Fako, F. Krumeich, R. Hauert, O. V. Safonova, V. A. Kondratenko, E. V. Kondratenko, S. M. Collins, P. A. Midgley, N. López, J. Pérez-Ramírez, *Chem. Sci.* **2019**, *10*, 359.
- [30] H. Liu, Y. Zhang, R. Li, X. Sun, S. Desilets, H. Abou-Rachid, M. Jaidann, L.-S. Lussier, *Carbon* **2010**, *48*, 1498.
- [31] S. N. Nesov, P. M. Korusenko, V. V. Bolotov, S. N. Povoroznyuk, D. A. Smirnov, *Phys. Solid State* **2017**, *59*, 2030.
- [32] D. Geng, S. Yang, Y. Zhang, J. Yang, J. Liu, R. Li, T.-K. Sham, X. Sun, S. Ye, S. Knights, *Appl. Surf. Sci.* **2011**, *257*, 9193.
- [33] P. M. Korusenko, V. V. Bolotov, S. N. Nesov, S. N. Povoroznyuk, I. P. Khailov, *Nucl. Instrum. Methods B* **2015**, *358*, 131.
- [34] M. V. Ivanova, C. Lamprecht, M. J. Loureiro, J. T. Huzil, M. Foldvari, *Int. J. Nanomed.* **2012**, *7*, 403.
- [35] Z. Song, W. Liu, N. Cheng, M. N. Banis, X. Li, Q. Sun, B. Xiao, Y. Liu, A. Lushington, R. Li, L. Liu, X. Sun, *Mater. Horiz.* **2017**, *4*, 900.
- [36] D. M. Basko, S. Piskanec, A. C. Ferrari, *Phys. Rev. B* **2009**, *80*, 165413.
- [37] R. Saito, M. Hofmann, G. Dresselhaus, A. Jorio, M. S. Dresselhaus, *Adv. Phys.* **2011**, *60*, 413.
- [38] Z. Zhang, Y. Chen, L. Zhou, C. Chen, Z. Han, B. Zhang, Q. Wu, L. Yang, L. Du, Y. Bu, P. Wang, X. Wang, H. Yang, Z. Hu, *Nat. Commun.* **2019**, *10*, 1657.
- [39] H. Wei, K. Huang, D. Wang, R. Zhang, B. Ge, J. Ma, B. Wen, S. Zhang, Q. Li, M. Lei, C. Zhang, J. Irawan, L.-M. Liu, H. Wu, *Nat. Commun.* **2017**, *8*, 1490.
- [40] T. Li, J. Liu, Y. Song, F. Wang, *ACS Catal.* **2018**, *8*, 8450.
- [41] P. H.-L. Sit, R. Car, M. H. Cohen, A. Selloni, *Inorg. Chem.* **2011**, *50*, 10259.
- [42] L. G. Bulusheva, A. V. Okotrub, A. G. Kurennya, H. Zhang, H. Zhang, X. Chen, H. Song, *Carbon* **2011**, *49*, 4013.
- [43] A. R. MacIntosh, G. Jiang, P. Zamani, Z. Song, A. Riese, K. J. Harris, X. Fu, Z. Chen, X. Sun, G. R. Goward, *J. Phys. Chem. C* **2018**, *122*, 6593.
- [44] J. VandeVondele, M. Krack, F. Mohamed, M. Parrinello, T. Chassaing, J. Hutter, *Comput. Phys. Commun.* **2005**, *167*, 103.
- [45] J. Tao, J. P. Perdew, V. N. Staroverov, G. E. Scuseria, *Phys. Rev. Lett.* **2003**, *91*, 146401.
- [46] C. Hartwigsen, S. Goedecker, J. Hutter, *Phys. Rev. B* **1998**, *58*, 3641.
- [47] J. VandeVondele, J. Hutter, *J. Chem. Phys.* **2007**, *127*, 114105.
- [48] J. K. Nørskov, T. Bligaard, A. Logadottir, J. R. Kitchin, J. G. Chen, S. Pandalov, U. Stimming, *J. Electrochem. Soc.* **2005**, *152*, J23.